Brief Communication: Initializing RAMMS with High Resolution LiDAR Data for Avalanche Simulations

James Dillon [1] and Kevin Hammonds [1]

[1]Department of Civil Engineering, Montana State University, Bozeman, MT 59717, USA

Correspondence: James Dillon (james.dillon013@gmail.com) & Kevin Hammonds (kevin.hammonds@montana.edu)

Abstract. The Rapid Mass Movements Simulator (RAMMS) is an avalanche dynamics software tool for research and forecasting. Since the model's conception, the sensitivity of inputs on simulation results has been well-documented. Here, we introduce a new method for initializing RAMMS that can be easily operationalized for avalanche forecasting using high resolution LiDAR data. As a demonstration, hypothetical avalanche simulations were performed while incrementally incorporating

5 semi-automated LiDAR-derived values for snow depth, interface topography, and vegetative cover from field-collected LiDAR data. Results show considerable variation in the calculated runout extent, flow volume, pressure, and velocity of the simulated avalanches when incorporating these LiDAR-derived values.

1 Introduction

The Rapid Mass Movements Simulator (RAMMS) is a unique avalanche simulation toolbox, which models flow depth, veloc-

10 ity, impact pressure, and run-out distance based on a depth-averaged hydrodynamic system of equations with a Voellmy-Salm friction relation (Christen et al., 2010b; Salm, 1993). In a typical application of RAMMS, a user will 1) input a digital elevation model (DEM) of the underlying ground surface, 2) assign an avalanche start-zone based on local expertise or a GIS-based terrain analysis (Maggioni and Gruber, 2003), 3) provide an estimate of start-zone snow depth using in situ and/or automated weather station observations, and 4) delineate vegetated areas if necessary, typically from photographs or a separate database.

15 Additional parameters such as snow density, Coloumb friction, and viscous resistance can be assigned as well. Once ingested into RAMMS, the fine-tuning of these inputs is imperative in obtaining a realistic result, as first noted by Christen et al. (2010b). For instance, Bühler et al. (2011) demonstrated significantly different outputs from RAMMS by simply varying the spatial resolution of the input DEM, while Fischer et al. (2012) noted that centrifugal forces arising from the curvature of the local terrain can also have significant impacts on the simulated acceleration of the avalanche and the frictional response.

20 Here, we introduce a new method for initializing RAMMS for operational avalanche forecasting using high-spatial resolution LiDAR data. With these data, common DEM's are replaced with surface models from LiDAR data point clouds gathered from either the bare ground or a previously exposed snow surface. Provided that repeat LiDAR scans were conducted throughout the winter period of snow accumulation, this allows avalanche forecasters the capability of choosing a sliding surface that can be either the snow-ground or a snow-snow interface of concern, perhaps due to the presence of a known weak layer.

25 With this approach, the topography of the snow-snow interface can be accounted for, which can vary substantially depending

on meteorological conditions or previous avalanche activity. Once the sliding surface has been chosen, any of the following LiDAR scans can be used as the input for snow depth, accounting for both the spatial variability in snow depth and the actual vegetative cover emergent from the sliding layer with a high degree of precision. Thus, with a minimum of two sequential LiDAR scans, the typically assumed or generic inputs used for RAMMS (i.e. the DEM, snow depth, and vegetative cover)
30   can be replaced with actual observations of high spatial and temporal resolution, potentially creating a more realistic RAMMS simulation for guiding avalanche forecasting and mitigation efforts.

2   Background

When evaluating previous studies using RAMMS for avalanche forecasting applications (Bühler et al., 2011; Christen et al., 2010a; Harvey et al., 2018), it was found that users would commonly assign a uniform snow depth to an avalanche starting
35   zone, neglecting to account for the spatial variability in snow depth atop the sliding surface, which can dramatically alter release volume (Deems et al., 2015). Given that there always exists some spatial variability in snow depth in natural snow covers (e.g., Seligman et al., 1936; Birkeland et al., 1995; Schweizer et al., 2008), particularly in wind-affected mountainous regions (Hiemstra et al., 2002), it is expected that this would produce error in the simulation. For instance, in Maggioni et al. (2012), where the accuracy of RAMMS was evaluated from real avalanche events, the authors used a single observation of
40   new snow depth as their uniform start-zone snow depth, but noted considerable variability in the subsequent avalanche crown height. Similarly, although Christen et al. (2010a) accounted for this variability in their observed avalanche back-calculation, by adding or subtracting snow depth from a central value based on slope aspect and observations of wind speed and direction, this is simply not practical in a more operational environment. Furthermore, there also exists spatial variability in terrain curvature and interface topography (i.e. snow-snow vs. snow-ground interface topography) as observed in Veitinger and Sovilla (2016).
45   They showed that snow surfaces tend to have fewer fine-scale irregularities than their underlying ground surface. Based on these previous studies, it is reasonable to expect the slope angle and curvature at a given snow-snow interface to also be spatially variable and perhaps not representative of the underlying ground surface, further affecting the accuracy of RAMMS calculations if only using a ground-based DEM for the sliding surface topography. Towards accounting for both the spatial variability in snow depth and interface topography, LiDAR has demonstrated capacity in generating high-spatial resolution
50   maps of both surface elevation and snow depth, be it total snow depth or new snow accumulation atop older layers of snow (Deems et al., 2015; Painter et al., 2016). Therefore, due to the well-documented importance of spatial variability for avalanche release (Schweizer et al., 2008), LiDAR presents itself as a logical alternative for assigning sliding topography and snow depth in RAMMS, as opposed to using uniform snow depth estimates derived from meteorological observations or point measurements.
55   In addition to accounting for snow deposition, LiDAR also has the capacity to delineate vegetation relevant to avalanche modelling in a precise manner. As mentioned above, vegetated areas are typically identified from photography, local knowledge, or an external dataset, then manually assigned to RAMMS as an input. However, vegetation completely buried beneath the sliding interface is irrelevant to the flow dynamics above the interface, such that it may not always be necessary to include.

A LiDAR scan of a future sliding interface prior to burial can yield detailed data on emergent, and thus obstructive, vegetation.

60 When generating a DEM from a LiDAR point cloud, points coincident with vegetation need to be delineated and excluded prior to interpolation in order to produce an accurate depiction of the ground (or snow layer) surface. Several techniques to achieve this delineation already exist for LiDAR, like the Riegl RiScan spatial vegetation filter used in this study. Therefore, high-spatial resolution maps of emergent vegetation from a buried interface can be extracted and transferred to RAMMS as an input, better accounting for spatial and temporal variability and removing the need for manual assignment.

3 Simulations

65

Four sets of four parallel RAMMS simulations were conducted using LiDAR data collected from avalanche terrain at the Yellowstone Club Ski Resort (YC), near Big Sky, MT, USA, during the 2019-2020 winter period. LiDAR scans were sequentially collected using a Riegl VZ-6000 terrestrial laser scanning LiDAR on four different outings, resulting in a ground scan (i.e. snow-off) and two on-snow scans, each with a varying depth, termed low-snow and high-snow, all of which are available at

70 https://doi.org/10.5061/dryad.z8w9ghx9z. The actual average snow depths for these cases were 0.13 and 1.35 m, respectively. Figure 1 shows an example of the variable snow depth measured via LiDAR on 12 March 2020.
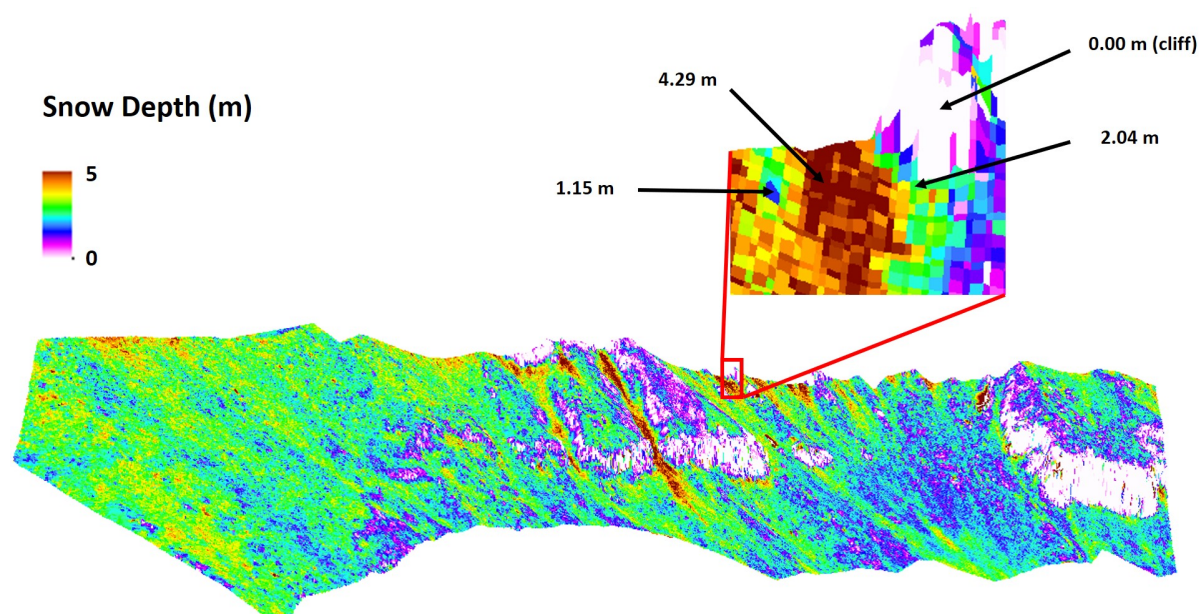

Figure 1. A map of total snow depth at the YC from 12 March 2020. The inset region shows considerable spatial variability in snow depth. Spatial resolution is 1 m.

Using our LiDAR datasets from the YC, a hypothetical avalanche event was simulated, where the topography of the low-snow layer was used as the sliding surface for an avalanche from the high-snow depth layer. Avalanche simulations were run at two different locations within the scans, one featuring ravines and gullies compared to another with relatively open slopes,

75   termed upper and lower (in reference to their location on the ridgeline), respectively. Point clouds were aligned by using
reflectors as tie points in Riegl's RiScan software. To create the required inputs for RAMMS, DEMs were generated for all
three scans with a spatial resolution of 1 m in ESRI's ArcMap 10.7.1, and then the low-snow layer subtracted from the high-
snow layer to delineate the spatial variability in snow depth atop the low-snow layer interface. It should be noted that this 1 m
resolution used for the simulations was the average of multiple LiDAR returns within a square meter, such that our simulations
80   account for fine-scale irregularities in both ground and snow surface topography. Four simulations were then performed with
additional LiDAR-derived data incorporated incrementally.

In Simulation 1, "traditional" inputs were used, assigning a ground DEM as the sliding layer, a uniform snow depth across the
entire start-zone, and a vegetated area delineated manually from photographs. The uniform snow depth applied was calculated
as the average snow depth atop the low-snow layer, which was 1.31 and 1.27 meters at the upper and lower sites, respectively.
85   In Simulation 2, the exact same parameters were used as in Simulation 1, but the low-snow layer was used as the sliding
interface, accounting for topographic variation due to variable snow deposition. In Simulation 3, a non-uniform snow depth
was incorporated, accounting for the actual spatial variability in snow depth. Whereas in Simulation 4, the same parameters as
in Simulation 3 were used, but the high-resolution emergent vegetation was mapped as well, instead of manually assigning this
from photographs. As shown in Figure 2, for the set of Simulations 1-4 on the upper site, it can be clearly discerned how the
90   incorporation of high-resolution LiDAR data into RAMMS can affect the initial conditions of the simulation. All other input
parameters were held constant across all simulations, including the snow density (300 kg/m3) and the momentum threshold
stopping criteria (5 percent). Friction coefficients were calculated using the automated workflow in RAMMS. Release volume,
maximum velocity, maximum flow height, and maximum pressure were then tabulated from each simulation. The resulting
simulations produced avalanches where the runout distance exceeded the LiDAR field-of-view, and thus we duplicated our
95   efforts with increased friction coefficient values that were manually assigned, as well as a stopping threshold criteria of 10
percent, to allow for observations of runout extent as it varied with the incorporation of LiDAR data. The increased friction
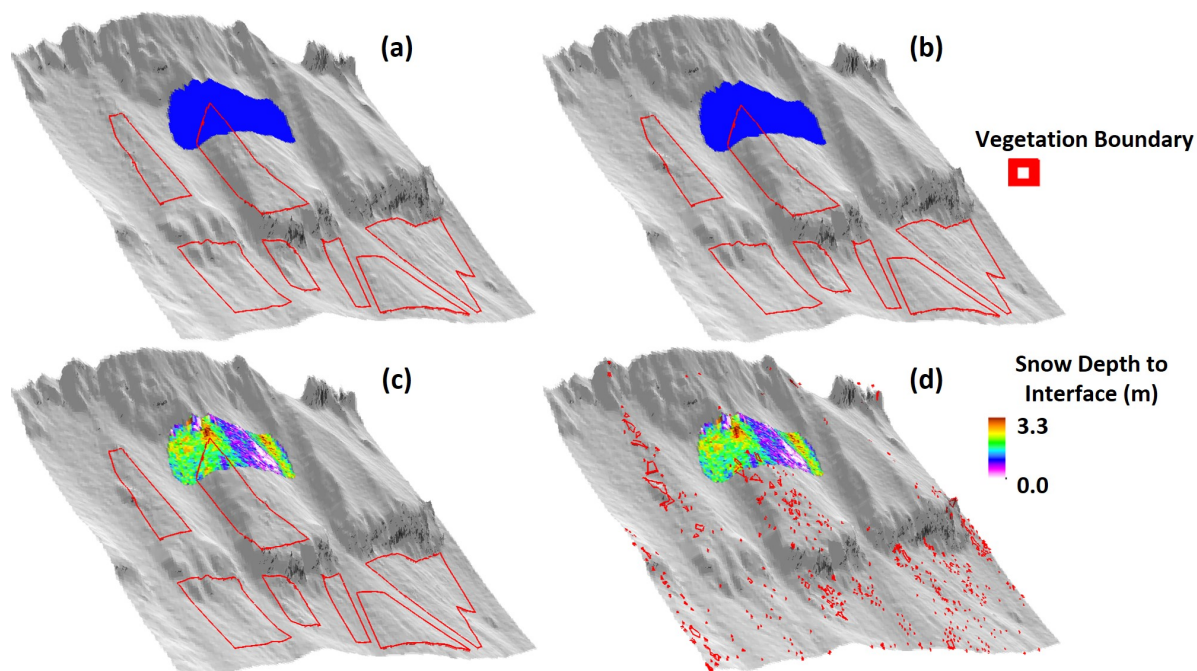coefficients were calculated by simply adding a constant value of 0.4 to the table of automatically generated values.

Figure 2. Comparison of RAMMS inputs between Simulations 1-4 at the upper site (a – d, respectively).

4 Results

Quantitative results are given in Table 1, where U1-U4 and L1-L4 are the results for the upper and lower sites, respectively.
Simulations with an asterisk (e.g. U1*) refer to simulations where manually increased friction coefficient values were used to
observe the runout extent. Animated simulations are also available for download at the repository mentioned in Section 3. Of
interest in these results, is that although the release volume did not change significantly in Simulations 2-4, when compared to
Simulation 1, the maximum velocity, flow height, and pressure varied substantially. Trends were reasonably similar between
sites; the introduction of the sliding layer DEM tended to decrease maximum velocity and pressure, while incorporating emer-
gent vegetation from LiDAR data had the opposite effect. Runout distance also varied substantially in the simulations with
increased friction coefficients. For instance, the maximum runout distance in U4 was 28 meters longer than that of U1, as
shown in Figure 3.

5 Discussion

The hypothetical avalanche simulations presented here demonstrate the considerable effect that model inputs have on RAMMS
simulation outputs, as originally noted by Christen et al. (2010b). However, we show that with high-spatial resolution LiDAR
data, more realistic inputs for RAMMS can be derived in a semi-automated manner. Consistent with the findings of Bühler
et al. (2011), we found that subtle variations in DEM topography can drastically impact simulation results, suggesting that

5

Simulation	Release Volume (m^3)	Δ (%)	Max Velocity (ms^{-1})	Δ (%)	Max Flow Height (m)	Δ (%)	Max Pressure (kPa)	Δ (%)	Runout Distance (m)	Δ (%)
U1	5699	–	34.7	–	5.9	–	362	–	–	
U2	5683	-0.3	25.6	-26.2	8.5	44.1	196	-45.9	–	–
U3	5515	-3.2	28.2	-18.7	8.3	40.7	238	-34.3	–	–
U4	5515	-3.2	33.1	-4.6	8.3	40.7	329	-9.1	–	–
U1*	–	–	14.9	–	5.0	–	67	–	129	–
U2*	–	–	13.6	-8.7	5.6	12.0	52	-22.4	130	0.8
U3*	–	–	12.3	-17.4	4.9	-2.0	45	-32.8	135	4.4
U4*	–	–	13.0	-12.8	4.9	-2.0	51	-23.9	157	17.8
L1	2304	–	19.8	–	2.3	–	118	–	–	–
L2	2317	0.6	17.7	-10.6	3.3	30.3	94	-20.3	–	–
L3	2285	-0.8	17.6	-11.1	3.2	28.1	93	-21.2	–	–
L4	2286	-0.8	20.7	4.4	2.9	20.7	128	7.8	–	–
L1*	–	–	7.1	–	1.8	–	15	–	131	–
L2*	–	–	7.1	0.0	2.3	21.7	15	0.0	146	10.3
L3*	–	–	7.1	0.0	2.5	28.0	15	0.0	147	10.9
L4*	–	–	7.6	6.6	2.5	28.0	17	11.8	156	16.0

Table 1. Quantitative results from RAMMS simulations, showing percent change when compared to traditional inputs used in Simulation 1. U1-U4 and L1-L4 designate the upper and lower site simulations, respectively. Asterisks denote simulations with a manually increased friction coefficient to observe runout distance.

accounting for the topography of the snow-snow interface is likely also important when avalanches slide above the base of the snowpack. This is illustrated in the data shown in Table 1, where a decrease in the maximum velocity was observed for

115 simulations that included the snow surface as the sliding surface (U2-U4, L2-L4), as opposed to the ground surface (U1, L1) in nearly all cases. Although somewhat counterintuitive, we note that in the upper site case, this is due to the subtle decrease in the slope angle ($\approx 5°$) of the sliding surface above the point of the maximum recorded velocity, which typically occurred in the couloir-like feature at mid-slope in the images shown in Figure 2. While it might be expected that a snow cover would provide a smoother and thus faster surface for avalanche flow, we observe here that a more smooth surface is not the only

120 relevant factor that snow surfaces can contribute towards the input DEM; slope angle and curvature can be altered as well, which are both fundamental to the resultant output of RAMMS. As has been noted in Veitinger and Sovilla (2016), variable snow accumulation and redistribution can reshape topography in site-specific ways, which is observed here.
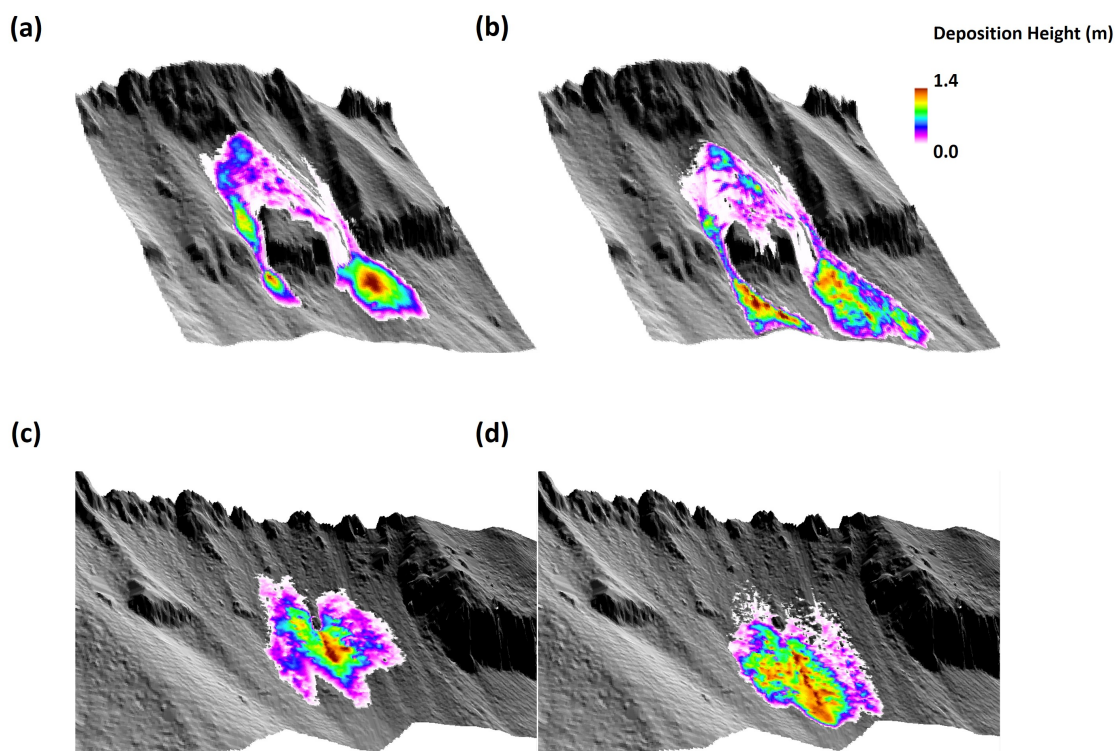
Figure 3. Final deposition height and runout extent of U1 (a), U4 (b), L1 (c), and L4 (d) with manually increased friction coefficients.

Although our results did not demonstrate significant variation in simulation outputs after the introduction of variable snow depth relative to a uniform snow depth in the start-zone, this is most likely due to the fact that we used the LiDAR-derived mean snow depth for assigning the uniform snow depth. In doing this, we indirectly accounted for the spatial variability in snow depth, adequately representing the total snow volume as an averaged value. However, without the LiDAR data to begin with, this would not have been possible. Accounting for vegetation that was emergent from an interface of interest and disregarding flora buried beneath also proved to be a relevant consideration, where an increase in maximum velocity, runout distance, and pressure was observed at both simulation sites.

As shown in previous work (Stoffel et al., 2018), it was determined that the operational implementation of RAMMS would require further study and potential modifications prior to being broadly implemented as an avalanche forecasting tool, while perhaps providing preliminary guidance in the interim. Based on the results shown here, we suggest that LiDAR data initialization holds the potential to dramatically improve the performance of RAMMS, although further investigation would be required before being implemented in an operational setting. In working towards operationalization for avalanche forecasting efforts, we suggest that if LiDAR data can be collected sequentially throughout a winter season, then LiDAR-derived DEMs corresponding to potential weak layers may be available for later RAMMS simulations to be executed upon. This would also allow for high-spatial resolution mapping of snow depth atop various snow-snow interfaces throughout the season. Similarly,

maps of emergent vegetation could also be generated after each snowfall event, further supporting later avalanche simulation and forecasting efforts by neglecting the effects of vegetation that has become buried.

140   In future work, we suggest that back-calculations of well-documented avalanche events that are coincident with LiDAR data collected throughout the winter season be performed, such that known bed surfaces and weak layers can be used for initializing RAMMS and comparing to field observations. Such a study would help discern whether or not LiDAR data initialization is truly of benefit to RAMMS, or conversely, if it is the further development of RAMMS that is necessary to make use of such detailed data inputs. Regardless, our results suggest that further research on the topic is merited, which would ultimately also be to the

145 benefit of any other depth-averaged avalanche dynamics and flow models that are developed in the future. For instance, Li et al. (2020) have recently demonstrated the capability of simulating various avalanche flow regimes in their dynamic avalanche flow model (Gaume et al., 2019), as well as showing a dependency of avalanche flow and deposition behavior on the runout angle. Should models such as these ever be implemented operationally at the hillslope scale, we suggest that the utility of these models also be investigated with LiDAR-derived inputs as well.

6 Data Availability

150

If accepted, data will be made available at https://doi.org/10.5061/dryad.z8w9ghx9z. Individual access during review is available upon request.

7 Author Contributions

KH was responsible for conceptualization, funding acquisition, project administration, resource procurement, supervision, and

155 reviewing and editing the draft manuscript. JD was responsible for investigation, formal analysis, visualization, and writing the initial draft manuscript.

8 Competing Interests

The authors declare that they have no conflict of interest.

9 Acknowledgements

References

Birkeland, K., Hansen, K., and Brown, R.: The spatial variability of snow resistance on potential avalanche slopes, Journal of Glaciology, 41, 183–190, 1995.

170 Bühler, Y., Christen, M., Kowalski, J., and Bartelt, P.: Sensitivity of snow avalanche simulations to digital elevation model quality and resolution, Annals of Glaciology, 52, 72–80, 2011.

Christen, M., Bartelt, P., and Kowalski, J.: Back calculation of the In den Arelen avalanche with RAMMS: interpretation of model results, Annals of Glaciology, 51, 161–168, 2010a.

Christen, M., Kowalski, J., and Bartelt, P.: RAMMS: Numerical simulation of dense snow avalanches in three-dimensional terrain, Cold

175 Regions Science and Technology, 63, 1–14, 2010b.

Deems, J. S., Gadomski, P. J., Vellone, D., Evanczyk, R., LeWinter, A. L., Birkeland, K. W., and Finnegan, D. C.: Mapping starting zone snow depth with a ground-based lidar to assist avalanche control and forecasting, Cold Regions Science and Technology, 120, 197–204, 2015.

Fischer, J.-T., Kowalski, J., and Pudasaini, S. P.: Topographic curvature effects in applied avalanche modeling, Cold Regions Science and

180 Technology, 74, 21–30, 2012.

Gaume, J., van Herwijnen, A., Gast, T., Teran, J., and Jiang, C.: Investigating the release and flow of snow avalanches at the slope-scale using a unified model based on the material point method, Cold Regions Science and Technology, 168, 102 847, 2019.

Harvey, S., Schmudlach, G., Bühler, Y., Dürr, L., Stoffel, A., and Christen, M.: Avalanche terrain maps for backcountry skiing in Switzerland, in: Proceedings of the International Snow Science Workshop, 07–12 October 2018, Innsbruck, Austria, pp. 1625–1631, 2018.

185 Hiemstra, C. A., Liston, G. E., and Reiners, W. A.: Snow redistribution by wind and interactions with vegetation at upper treeline in the Medicine Bow Mountains, Wyoming, USA, Arctic, Antarctic, and Alpine Research, 34, 262–273, 2002.

Li, X., Sovilla, B., Jiang, C., and Gaume, J.: The mechanical origin of snow avalanche dynamics and flow regime transitions, The Cryosphere, 14, 3381–3398, 2020.

Maggioni, M. and Gruber, U.: The influence of topographic parameters on avalanche release dimension and frequency, Cold Regions Science

190 and Technology, 37, 407–419, 2003.

Maggioni, M., Freppaz, M., Christen, M., Bartelt, P., and Zanini, E.: Back-calculation of small avalanches with the 2D avalanche dynamics model RAMMS: four events artificially triggered at the Seehore test site in Aosta Valley (NW-Italy), in: Proceedings of the International Snow Science Workshop, 16–21 September 2012, Anchorage, Alaska, pp. 591–598, 2012.

Painter, T. H., Berisford, D. F., Boardman, J. W., Bormann, K. J., Deems, J. S., Gehrke, F., Hedrick, A., Joyce, M., Laidlaw, R., Marks, D.,

195 et al.: The Airborne Snow Observatory: Fusion of scanning lidar, imaging spectrometer, and physically-based modeling for mapping snow water equivalent and snow albedo, Remote Sensing of Environment, 184, 139–152, 2016.

Salm, B.: Flow, flow transition and runout distances of flowing avalanches, Annals of Glaciology, 18, 221–226, 1993.

Schweizer, J., Kronholm, K., Jamieson, J. B., and Birkeland, K. W.: Review of spatial variability of snowpack properties and its importance for avalanche formation, Cold Regions Science and Technology, 51, 253–272, 2008.

200 Seligman, G., Seligman, G. A., and Douglas, C.: Snow structure and ski fields: being an account of snow and ice forms met with in nature, and a study on avalanches and snowcraft, Macmillan and Company, limited, 1936.

The Cryosphere
Discussions

Open Access

EGU

Stoffel, L., Bartelt, P., Margreth, S., and Schweizer, J.: Can Scenario-based avalanche dynamics calculations help in the decision making process for road closures?, in: Proceedings of the International Snow Science Workshop, 07–12 October 2018, Innsbruck, Austria, pp. 772–777, 2018.

205 Veitinger, J. and Sovilla, B.: Linking snow depth to avalanche release area size: measurements from the Vallée de la Sionne field site., Natural Hazards & Earth System Sciences, 16, 1953–1965, 2016.